CD57+ memory T cells proliferate in vivo

Raya Ahmed[1,*], Kelly L. Miners[2,*], Julio Lahoz-Beneytez[3,*], Rhiannon E. Jones[4], Laureline Roger[2], Christina Baboonian[1], Yan Zhang[1], Eddie C. Y. Wang[2], Marc K. Hellerstein[5], Joseph M. McCune[6], Duncan M. Baird[4], David A. Price[2,7,*], Derek C. Macallan[1,8,*], Becca Asquith[3,*], Kristin Ladell[2,9,*]

[1]Institute for Infection and Immunity, St. George's, University of London, London SW17 0RE, UK; [2]Division of Infection and Immunity, Cardiff University School of Medicine, Heath Park, Cardiff CF14 4XN, UK; [3]Department of Infectious Disease, Imperial College London, London W2 1PG, UK; [4]Division of Cancer and Genetics, Cardiff University School of Medicine, Heath Park, Cardiff CF14 4XN, UK; [5]Department of Nutritional Sciences and Toxicology, University of California Berkeley, CA 94720, USA; [6]HIV Frontiers Program, Global Health Innovative Technology Solutions, Bill & Melinda Gates Foundation, Seattle, WA 98109, USA; [7]Systems Immunity Research Institute, Cardiff University School of Medicine, Heath Park, Cardiff CF14 4XN, UK; [8]St George's University Hospitals NHS Foundation Trust, London SW17 0QT, UK; [9]Neonatal Unit, Singleton Hospital, Swansea Bay University Health Board, Swansea, SA2 8QA, UK.

*These authors contributed equally to this study.

Correspondence should be addressed to David A. Price (priced6@cardiff.ac.uk), Derek C. Macallan (macallan@sgul.ac.uk), Becca Asquith (b.asquith@imperial.ac.uk), or Kristin Ladell (ladellk@gmail.com).

Lead contact: Kristin Ladell (ladellk@gmail.com)

Running Title

CD57+ memory T cells proliferate in vivo

Key Points

CD57+ memory T cells are not replicatively senescent in vivo.

CD57+ memory T cells are maintained primarily via intracompartmental proliferation in vivo.

SUMMARY

A central paradigm in the field of lymphocyte biology asserts that replicatively senescent memory T cells express the carbohydrate epitope CD57. These cells nonetheless accumulate with age and expand numerically in response to persistent antigenic stimulation. We used in vivo deuterium labeling and ex vivo analyses of telomere length, telomerase activity, and intracellular expression of the cell-cycle marker Ki67 to distinguish between two non-exclusive scenarios: (i) CD57$^+$ memory T cells do not proliferate and instead arise via phenotypic transition from the CD57$^-$ memory T cell pool; and/or (ii) CD57$^+$ memory T cells self-renew via intracompartmental proliferation. Our results provide compelling evidence in favor of the latter scenario and further suggest in conjunction with mathematical modeling that self-renewal is by far the most abundant source of newly generated CD57$^+$ memory T cells. Immunological memory therefore appears to be intrinsically sustainable among highly differentiated subsets of T cells that express CD57.

INTRODUCTION

Immune senescence has been linked with the accumulation of terminally differentiated lymphocytes that fail to proliferate in response to antigenic challenge. It has also been suggested that surface expression of CD57, a terminally sulfated glycan carbohydrate epitope (Abo and Balch, 1981), identifies memory T cells that lack the capacity to proliferate (Brenchley et al., 2003). In line with these widely accepted paradigms, highly differentiated effector memory T cells that express CD45RA, known as T_{EMRA} cells, become more prevalent with age (Nociari et al., 1999) and often express CD57 (Ladell et al., 2008).

Contrary to the notion of differentiation-linked senescence, memory T cells that express CD57 can be induced to proliferate in vitro, at least under optimized conditions (Chong et al., 2008; Izquierdo et al., 1990). Parallel strands of evidence have further suggested a key role for these cells as immune effectors. For example, memory CD8^{+} T cells rarely express CD57 in conjunction with programmed death-1 (PD-1) (Petrovas et al., 2009), a marker associated with exhaustion (Day et al., 2006; Freeman et al., 2006; Petrovas et al., 2006; Trautmann et al., 2006), and functionally replete memory CD4^{+} and CD8^{+} T cells with cytotoxic potential typically express high levels of CD57 (Casazza et al., 2006; Chattopadhyay et al., 2009; Chong et al., 2008; Kern et al., 1999; Le Priol et al., 2006; Takata and Takiguchi, 2006; van Leeuwen et al., 2002). Virus-specific memory T cells have also been identified in the T_{EMRA} compartment (Appay et al., 2008). In the CD8^{+} lineage, these cells have been associated with protective effects, most notably during acute (Northfield et al., 2007) and chronic human immunodeficiency virus type 1 (HIV-1) infection (Addo et al., 2007), and in a study of elite controllers with eventual disease progession, increasing levels of viral replication appeared to drive the formation of CD28^{−}CD57^{+} memory CD8^{+} T cells, potentially indicating a reactive escalation in the cytotoxic response to HIV-1 (Benito et al., 2018). Accordingly, CD57^{+} memory T cells enrich the immune system with important antigen-dependent effector functions and, by extension, do not necessarily represent an irrelevant 'cul-de-sac' in the lymphocyte differentiation pathway.

In this study, we used deuterium labeling to quantify the proliferation of CD57$^-$ and CD57$^+$ memory T cells in vivo and supplemented these analyses with ex vivo measurements of telomere length, telomerase activity, and intracellular expression of the cell-cycle marker Ki67. We then used mathematical modeling to evaluate two non-exclusive hypothetical scenarios: (i) CD57$^+$ memory T cells arise from the CD57$^-$ memory T cell compartment as a consequence of progressive differentiation; and/or (ii) CD57$^+$ memory T cells self-renew via intracompartmental proliferation and thereby contribute to long-term immunological memory.

RESULTS

CD57⁻ and CD57⁺ memory T cells exhibit similar rates of deuterium incorporation

Preliminary in vivo labeling data were derived from studies of volunteers with chronic HIV-1 infection (aged 36–53 years), all of whom were antiretroviral drug-free at the time of experimentation and seropositive for cytomegalovirus (CMV; n = 4; Table S1). The labeling protocol is outlined in Figure 1A. Venous blood was sampled at weeks 7 (end of labeling), 10, 14, and 18, and at each time point, CD57⁻ and CD57⁺ memory CD8⁺ T cells were flow-sorted from the CD45RA⁻CCR7⁻ subset at >98% purity (Figure S1). This gating strategy was designed to exclude T_{EMRA} cells, which were assessed separately in an earlier report (Ladell et al., 2008). Considerable rates of ^2H labeling and delabeling were observed among CD45RA⁻CCR7⁻CD57⁻ and CD45RA⁻CCR7⁻CD57⁺ memory CD8⁺ T cells (Figure 1B).

Immune activation enhances the turnover of memory T cells in the setting of chronic HIV-1 or HIV-2 infection (Hegedus et al., 2014; McCune et al., 2000; Vrisekoop et al., 2015; Zhang et al., 2013). We therefore sought to confirm these preliminary findings in a more comprehensive labeling study of healthy volunteers (aged 29–83 years), all of whom were seronegative for HIV-1 and seropositive for CMV. Recruitment was stratified to include equal numbers of young (aged 29–47 years) and elderly individuals (aged 60–83 years), the latter representing a population in which immune senescence was more likely (total n = 8; Table S1). Venous blood was sampled during the labeling phase (weeks 1, 3, and 5), at the end of labeling (week 7), and during the delabeling phase (weeks 8, 10, 14, and 18) (Figure 1A). At each time point, CD57⁻ and CD57⁺ memory T cells were flow-sorted from the CD4⁺ and CD8⁺ lineages at >98% purity after gating out potentially naive CD27^bright CD45RO⁻ events (Figure 1C and Figure S1).

In each coreceptor-defined lineage, similar patterns of ^2H labeling and delabeling were observed among CD57⁻ and CD57⁺ memory T cells, and equivalent (n = 3) or greater rates of ^2H labeling (n = 5) were observed among CD57⁺ memory T cells compared with CD57⁻

5

memory T cells (Figure 1D and E). Importantly, the corresponding ^{2}H label enrichments in body water followed an expected rise-and-fall profile (Figure S2), and in the context of age-related immune senescence, no intralineage or intrasubset differences in the kinetics of ^{2}H accumulation or loss were apparent between young and elderly volunteers (Figure 1D and E).

Ki67$^+$ cells are readily detectable in the CD57$^+$ memory T cell pool

To corroborate these findings, we measured the expression of Ki67, an intracellular marker that accumulates during active phases of the cell cycle (Gerdes et al., 1983; Miller et al., 2018). Cytosolic expression of Ki67 was detected in the CD4$^+$ lineage at mean frequencies of 1% among CD57$^-$ memory T cells and 2.9% among CD57$^+$ memory T cells (p = 0.02, paired samples Wilcoxon test; Figure 2A and B) and in the CD8$^+$ lineage at mean frequencies of 0.7% among CD57$^-$ memory T cells and 0.4% among CD57$^+$ memory T cells (p = 0.008, paired samples Wilcoxon test; Figure 2A and B). Higher frequencies were observed using a different approach that simultaneously exposed intranuclear antigens. Cytosolic/nuclear expression of Ki67 was detected in the CD4$^+$ lineage at mean frequencies of 4.9% among CD57$^-$ memory T cells and 8.6% among CD57$^+$ memory T cells (p = 0.742, paired samples Wilcoxon test; Figure 2C and D) and in the CD8$^+$ lineage at mean frequencies of 1.2% among CD57$^-$ memory T cells and 1.9% among CD57$^+$ memory T cells (p = 0.039, paired samples Wilcoxon test; Figure 2E and F).

In further analyses, we assessed the phenotypic characteristics of Ki67$^+$CD57$^-$ and Ki67$^+$CD57$^+$ memory T cells in the CD4$^+$ and CD8$^+$ lineages. As expected, Ki67$^+$ memory CD4$^+$ T cells predominantly expressed CD45RO, with or without CD57, whereas Ki67$^+$ memory CD8$^+$ T cells were phenotypically more heterogeneous and often expressed CD45RA in conjunction with CD57 (Figure 2G). Moreover, Ki67$^+$CD57$^-$ memory T cells expressed CD28 at higher frequencies than Ki67$^+$CD57$^+$ memory T cells, both in the CD4$^+$ lineage (p = 0.008, paired samples Wilcoxon test; Figure 2D and H) and in the CD8$^+$ lineage

(p = 0.008, paired samples Wilcoxon test; Figure 2F and I). Similar patterns of expression were observed for CCR7 (Figure S3).

To link these findings with the labeling data, we compared the phenotypic characteristics of Ki67$^+$CD57$^-$ and Ki67$^+$CD57$^+$ memory T cells with the phenotypic characteristics of CD57$^-$ and CD57$^+$ memory T cells sampled from the healthy volunteers in Cohort 2. In both coreceptor-defined lineages, CD57$^-$ memory T cells expressed CD28 and CCR7 at higher frequencies than CD57$^+$ memory T cells, akin to the corresponding Ki67$^+$ memory T cells (Figure S4). Of note, CD57$^+$ memory CD4$^+$ T cells mostly lacked CD27 but commonly expressed CD127 and PD-1, whereas CD57$^+$ memory CD8$^+$ T cells were generally more differentiated and rarely expressed CD27, CD127, or PD-1 (Figures S4 and S5). Age had no apparent influence on these phenotypic characteristics (data not shown).

CD57$^-$ and CD57$^+$ memory T cells have similar division histories

To refine our understanding of these datasets, we measured XpYp or 17p telomere lengths in the CD57$^-$ and CD57$^+$ memory T cell pools (Figure 3A). Telomere lengths were distributed in a heterogeneous manner and overlapped considerably across CD57-defined subsets in the CD4$^+$ and CD8$^+$ lineages. In some volunteers, significant differences in mean telomere length were observed between the CD57$^-$ and CD57$^+$ memory T cell populations, most commonly in the CD4$^+$ lineage, but no consistent directional change was apparent between CD57-defined subsets in either the CD4$^+$ or the CD8$^+$ lineage (Figure 3B and C). However, pooling the XpYp data from labeled volunteers revealed that telomere lengths were maintained to a slightly greater extent in the CD57$^-$ memory CD4$^+$ T cell population compared with the CD57$^+$ memory CD4$^+$ T cell population (Figure 3D), and pooling the 17p data from volunteers in Cohort 3 yielded a similar result with borderline significance (p = 0.037, Mann-Whitney U test; data not shown). Telomerase activity was generally low, as expected given the infrequent expression of Ki67, but marginally higher levels were detected among CD57$^-$ memory T cells compared with CD57$^+$ memory T cells in both coreceptor-

defined lineages. These data were reported previously for reference in another labeling study of the volunteers in Cohort 2 (Ahmed et al., 2016).

CD57⁻ and CD57⁺ memory T cells self-renew in vivo

To integrate these findings, we fitted mathematical models simultaneously to the ^2H enrichment data and the telomere length data, allowing CD57⁻ memory T cells to become CD57⁺ memory T cells in the CD4⁺ and CD8⁺ lineages (Figure 4A). This approach was designed to capture both possible explanations for the accumulation of label in the corresponding CD57⁺ compartments, namely that CD57⁻ memory T cells proliferated and acquired expression of CD57 and/or that CD57⁺ memory T cells proliferated and retained expression of CD57. Proliferation rates were denoted by p_1 and p_2 for CD57⁻ and CD57⁺ memory T cells, respectively, such that replicative senescence in the CD57⁺ subsets was represented by the constraint $p_2 = 0$. Telomeres shorten by an average of 50 bp per cell division (De Boer and Noest, 1998). In some cases, this rate of erosion can be counteracted by the activity of telomerase, a possibility that was included in the model assumptions via an additional parameter, termed K.

Fits were restricted to the volunteers for whom labeling data and telomere length data were available (n = 5). The general model (with p_2 free) fitted the data well for CD57⁻ and CD57⁺ memory T cells in the CD4⁺ and CD8⁺ lineages (Figure 4B and Table 1). Importantly, the proliferation rate estimates for the CD57⁺ subsets were positive, with 95% confidence intervals that did not overlap zero (i.e., $p_2 > 0$). This conclusion was robust to different rates of telomere shortening per cell division and changes in the parameter K (Figure S6). Model performance was considerably worse if proliferation was disallowed in the CD57⁺ memory T cell populations (i.e., $p_2 = 0$) (Figures 4B and S7). Indeed, the median p value in a comparison of the models was 5×10^{-20} (F test), which provided strong evidence to reject the null hypothesis of the simpler model, namely that CD57⁺ memory T cells were unable to proliferate (i.e., $p_2 = 0$). Moreover, the median small-sample-corrected Akaike information

criterion (AICc) difference was 106, which indicated that the simpler model provided a substantially worse description of the data (i.e., fit after adjustment for model complexity). The best fits were therefore consistent with substantial proliferation in the CD57$^+$ compartments, such that influx from the CD57$^-$ compartments typically contributed only ~5% of all newly generated CD57$^+$ memory T cells (Table 1).

DISCUSSION

In this study, we used in vivo deuterium labeling and ex vivo analyses of telomere length, telomerase activity, and intracellular expression of the cell-cycle marker Ki67 to investigate the paradigm that replicatively senescent memory T cells can be identified via the surrogate marker CD57. We detected similar rates of proliferation among CD57$^-$ and CD57$^+$ memory T cells in both coreceptor-defined lineages. These results were supported by flow cytometric analyses, which revealed the presence of actively dividing cells in the corresponding CD57$^+$ memory T cell populations. Marginally higher levels of telomerase activity were detected among CD57$^-$ memory T cells compared with CD57$^+$ memory T cells in the CD4$^+$ and CD8$^+$ lineages, consistent with a relatively small biological effect, and in line with recent observations (Fali et al., 2018), telomere lengths were maintained to a slightly greater extent among CD57$^-$ memory CD4$^+$ T cells compared with CD57$^+$ memory CD4$^+$ T cells. In contrast, telomere lengths were distributed around similar means in the CD57$^-$ and CD57$^+$ memory CD8$^+$ T cell populations. Mathematical modeling of the experimental data further suggested that self-renewal via intracompartmental proliferation rather than replenishment via phenotypic conversion was by far the most abundant source of newly generated CD57$^+$ memory CD4$^+$ and CD57$^+$ memory CD8$^+$ T cells.

CD57 was originally recognized as a differentiation antigen on the surface of NK cells (Abo and Balch, 1981) and subsequently associated with other lymphocyte subsets in germinal centers (Ritchie et al., 1983). In peripheral blood, CD57$^+$ memory T cells accumulate throughout life, especially after infection with CMV (Gratama et al., 1989). These associations with age and persistent antigenic drive were mechanistically linked in a seminal in vitro study, which reported that replicatively senescent memory CD8$^+$ T cells expressed CD57 (Brenchley et al., 2003). However, an earlier study had reached a different conclusion (Izquierdo et al., 1990), and later experiments showed that CD57$^+$ memory CD8$^+$ T cells were able to proliferate in vitro in the presence of certain growth factors, potentially mimicking the in vivo microenvironment (Chong et al., 2008). Similar findings were reported

in another study, although markedly higher response frequencies on a per cell basis were noted in the CD57$^-$ subset compared with the CD57$^+$ subset (Le Priol et al., 2006). Nonetheless, the proportion of responding cells in the CD57$^+$ subset was more than sufficient to maintain homeostatic turnover, at least according to a deuterium labeling study of bulk memory T cell populations (Zhang et al., 2013).

T$_{EMRA}$ cells are somewhat resistant to apoptosis (Gupta et al., 2007) and retain deuterium in the CD8$^+$ lineage with an estimated half-life of approximately 25 years, assuming simple exponential decay without phenotypic conversion (Ladell et al., 2008). In response to extreme stimulation with supraphysiological concentrations of phytohemagglutinin and interleukin-2, CD8$^+$ T$_{EMRA}$ cells that expressed CD57 were recently found to be more susceptible to cell death than CD8$^+$ T$_{EMRA}$ cells that lacked CD57 (Verma et al., 2017). This observation was thought to indicate a functional dichotomy between CD57-defined subsets within the CD8$^+$ T$_{EMRA}$ compartment. However, it does not necessarily follow that a similar dichotomy exists under homeostatic conditions, because terminally differentiated CD57$^+$ memory CD8$^+$ T cells may be protected from excessive stimulation in vivo by a lack of costimulatory receptors, such as CD27 and CD28.

In summary, we have shown that CD57$^+$ memory T cells in the CD4$^+$ and CD8$^+$ lineages self-renew in vivo, enabling the long-term maintenance of functionally replete immunological memory. It remains to be determined how this process is regulated in terms of antigenic drive versus homeostatic signals as a function of differentiation status, but nonetheless, it is clear from the presented data that replicatively senescent memory T cells cannot be defined solely via surface expression of CD57.

CONTACT FOR REAGENT AND RESOURCE SHARING

Further information and requests for reagents and resources should be directed to and will be fulfilled by the Lead Contact, Kristin Ladell (ladellk@gmail.com).

EXPERIMENTAL MODEL AND SUBJECT DETAILS

Human participants

Three groups of human volunteers participated in this work. Cohort 1: volunteers with chronic HIV-1 infection (aged 36–53 years) were recruited for preliminary in vivo labeling studies (n = 4 males; Table S1). All were antiretroviral drug-free and seropositive for CMV. Cohort 2: healthy volunteers (aged 29–83 years) were recruited for more extensive in vivo labeling studies (n = 3 females; n = 5 males; Table S1). All were seronegative for hepatitis C virus and HIV-1 and seropositive for CMV. Cohort 3: additional healthy volunteers (aged 28–58 years) were recruited for phenotypic studies and measurements of telomere length and telomerase activity (n = 7 females; n = 7 males). Similar experiments were performed using venous blood samples donated by 5 of the 8 volunteers in Cohort 2. All studies were conducted in accordance with the principles of the Declaration of Helsinki. Ethical approval was granted by the University of California Committee on Human Research (Cohort 1), the London-Chelsea Research Ethics Committee (Cohort 2), and the Cardiff University School of Medicine Research Ethics Committee (Cohort 3).

METHOD DETAILS

Measurement and analysis of deuterium enrichment in T cell DNA

T cell proliferation in vivo was measured using deuterium (^{2}H) labeling as described previously (Busch et al., 2007; Hellerstein et al., 1999; Ladell et al., 2008; McCune et al., 2000; Neese et al., 2001; Westera et al., 2013). Briefly, volunteers received heavy water (^{2}H$_2$O) orally for 7 weeks (Figure 1A), and deuterium incorporation into the DNA of flow-sorted T cells was quantified via gas chromatography/mass spectrometry (Agilent 5873/6980) (Ladell et al., 2008). DNA was released by boiling and hydrolyzed according to standard protocols, and deoxyribonucleosides were derivatized using pentafluorobenzyl hydroxylamine (Sigma-Aldrich). Gas chromatography/mass spectrometry was performed in negative chemical ionization mode using a DB-17 column (Agilent). The M+1/M+0 isotopomer ratio was monitored at mass-to-charge (m/z) 436/435. To normalize for body water enrichment, weekly saliva samples were analyzed for ^{2}H$_2$O content via calcium carbide-induced acetylene generation, monitoring at m/z 27/26 (Previs et al., 1996).

Flow cytometry and cell sorting

T cell subsets of interest were flow-sorted from freshly isolated peripheral blood mononuclear cells (PBMCs) at >98% purity using a FACSVantage SE, a FACSAria, or a Special Order Research Product FACSAria II (all from BD Biosciences). Cells were stained with combinations of the following reagents: (i) anti-CD3–APC-H7 (clone SK7), anti-CD14–V500 (clone M5E2), anti-CD19–V500 (clone HIB19), anti-CD28–APC (clone CD28.2), anti-CD45RA–PE (clone HI100), and anti-CD57–FITC (clone NK-1) from BD Biosciences; (ii) anti-CD4–PE-Cy5.5 (clone S3.5), anti-CD27–QD605 (clone CLB-27/1), and LIVE/DEAD Fixable Aqua from Thermo Fisher Scientific; (iii) anti-CD8–BV711 (clone RPA-T8), anti-CD28–BV421 (clone CD28.2), anti-CD57–PE-Cy7 (clone NK-1), anti-CD127–BV421 (clone A019D5), anti-CCR7–PE-Cy7 (clone G043H7), anti-CXCR3–BV421 (clone G025H7), and anti-PD-1–BV421 (clone EH12.2H7) from BioLegend; and (iv) anti-CD45RO–ECD (clone UCHL1) from Beckman Coulter. Viable CD57$^-$ and CD57$^+$ memory T cells were identified in the CD4$^+$ and/or CD8$^+$ lineages after exclusion of CD27^{bright}CD45RO$^-$ (Figure 1C) or CD45RA$^+$CCR7$^+$ events (Figure S1). Cytosolic expression of Ki67 was evaluated using anti-

Ki67–AF647 (clone B56; BD Biosciences) in conjunction with a Cytofix/Cytoperm Kit (BD Biosciences), and cytosolic/intranuclear expression of Ki67 was evaluated using anti-Ki67–FITC (clone B56; BD Biosciences) in conjunction with a Foxp3 Transcription Factor Staining Buffer Kit (Thermo Fisher Scientific). Data were analyzed with FlowJo software version 9.9.4 (FlowJo LLC).

Single chromosome telomere length analysis

DNA was extracted from 3,000 flow-sorted T cells using a QIAmp DNA Micro Kit (Qiagen). Single telomere length analysis (STELA) was carried out at the XpYp or the 17p telomere as described previously (Capper et al., 2007). Briefly, 0.75 µL of the Telorette-2 linker (10 µM) was added to genomic DNA eluted in 35 µL of Tris (10 mM). Multiple PCRs were then performed for each test DNA. Each reaction was set up in a final volume of 10 µL containing 250 pg of DNA and the telomere-adjacent and Teltail primers at a final concentration of 0.5 µM in 75 mM Tris-HCl pH 8.8, 20 mM $(NH_4)_2SO_4$, 0.01% Tween-20, and 1.5 mM $MgCl_2$, with 0.5 U of a 10:1 mixture of Taq (Thermo Fisher Scientific) and Pwo polymerase (Sigma-Aldrich). The reactions were processed in a Tetrad2 Thermal Cycler (Bio-Rad). DNA fragments were resolved via 0.5% Tris-acetate-EDTA agarose gel electrophoresis and identified via Southern hybridization with a random-primed α-^{33}P-labeled (PerkinElmer) TTAGGG repeat probe, together with probes specific for molecular weight markers at 1 kb (Agilent) and 2.5 kb (Bio-Rad). Hybridized fragments were detected using a Typhoon FLA 9500 Phosphorimager (GE Healthcare). The molecular weights of the DNA fragments were calculated using Phoretix 1D Quantifier (Nonlinear Dynamics).

Measurement of telomerase activity

Flow-sorted T cells were lyzed and assayed in two steps using a modified SYBR Green real-time quantitative telomeric repeat amplification protocol (Wege et al., 2003). Standard curves were obtained from serial dilutions of a 293T cell extract with known telomerase

activity. Experimental telomerase activity was calculated with reference to 293T cells and expressed as relative telomerase activity (Ct_{293T}/Ct_{sample}).

QUANTIFICATION AND STATISTICAL ANALYSIS

General statistics

Unmatched groups were compared using the Mann-Whitney U test, and matched groups were compared using the paired samples Wilcoxon test. Significance was assigned at $p < 0.05$.

Mathematical modeling

Mechanistic ordinary differential equation-based models were developed to assess the dynamics of CD57$^-$ and CD57$^+$ memory T cells (Costa Del Amo et al., 2018; Patel et al., 2017). These subsets were modeled as dependent populations to investigate the possibility that label acquisition in the CD57$^+$ compartment was a consequence of proliferation-linked differentiation in the CD57$^-$ compartment. Accordingly, CD57$^-$ and CD57$^+$ memory T cells were allowed to proliferate and die or exit the circulation, and CD57$^-$ memory T cells were allowed to gain expression of CD57. The phenotypic conversion of CD57$^-$ memory T cells into CD57$^+$ memory T cells was considered over n rounds of division, including the possibility that $n = 0$.

In the applied model, CD57$^-$ memory T cells (x_1) became CD57$^+$ memory T cells (x_2) at a rate m:

$$\frac{dx_1}{dt} = p_1 x_1 - z_1 x_1$$

$$\frac{dx_2}{dt} = p_2 x_2 - z_2 x_2 + m x_1$$

where p_1 and p_2 are the rates of proliferation of CD57$^-$ and CD57$^+$ memory T cells, respectively, and z_1 and z_2 are the rates of disappearance of CD57$^-$ and CD57$^+$ memory T cells, respectively. The possibility that surface expression of CD57 could be acquired during clonal expansion was accommodated in the permitted values for m (bounds during fitting [0,40]).

To minimize the number of free parameters, label enrichment among CD57$^+$ memory T cells was assumed to originate either from dividing CD57$^-$ memory T cells that differentiated into CD57$^+$ memory T cells or from dividing CD57$^+$ memory T cells. A model in which the acquisition of CD57 was not coincident with clonal expansion resulted in a substantially worse fit to the data and was not pursued further. The fraction of label thus became:

$$\frac{dL_1}{dt} = p_1 b_w U_t - z_1^* L_1$$

$$\frac{dL_2}{dt} = (p_2 + mR) b_w U_t - z_2^* L_2$$

where p_1 and p_2 are as above, z_1^* and z_2^* are the rates of loss of labeled CD57$^-$ and CD57$^+$ memory T cells, respectively, L_1 and L_2 are the fractions of labeled deoxyadenosine among CD57$^-$ and CD57$^+$ memory T cells, respectively, R is the ratio of CD57$^-$ to CD57$^+$ memory T cells (x_1/x_2), and b_w is the amplification factor estimated from label acquisition among granulocytes, assuming 100% turnover in 7 weeks. Data were available from four volunteers and gave a population average value for b_w of 3.5, consistent with previous studies (Ahmed et al., 2015; Lahoz-Beneytez et al., 2016). The value of b_w was therefore fixed at 3.5. Finally, $U(t)$ is an empirical function used to describe the availability of label in body water:

$$U(t) = f(1 - e^{-\delta t}) + \beta e^{-\delta t} \qquad \text{during labeling } t \text{ £ } \tau$$

$$U(t) = [f(1 - e^{-\delta t}) + \beta e^{-\delta t}]e^{-\delta(t-\tau)} \qquad \text{after labeling } t > \tau$$

as described previously (Vrisekoop et al., 2008), where $U(t)$ represents the fraction of labeled precursor in body water at time t (in days), f is the fraction of labeled precursor in ingested water, τ is the length of the labeling period, δ is the turnover rate of body water per day, and β is the plasma enrichment attained at the end of day 0. Parameters were estimated by fitting the above functions to the deuterium labeling data measured in saliva. The resulting fits of $U(t)$ to saliva measurements are shown in Figure S2.

Inclusion of telomere length data in the model fits

The impact of cell division on telomere length was modeled as described previously (De Boer and Noest, 1998). Telomere length data were available for 5 of the 8 volunteers in Cohort 2. The model was fitted simultaneously to the labeling data and the telomere length data using the free parameters p_1 and p_2 to describe the rates of proliferation of CD57$^-$ and CD57$^+$ memory T cells, respectively, $z_1{}^*$ and $z_2{}^*$ to describe the rates of disappearance of labeled CD57$^-$ and CD57$^+$ memory T cells, respectively, and mR, the rate of conversion from CD57$^-$ to CD57$^+$ memory T cells (m) multiplied by the ratio of the frequency of CD57$^-$ memory T cells to the frequency of CD57$^+$ memory T cells (R).

Estimation of telomere length change

The rate of change in telomere loss indices for CD57$^-$ memory T cells was defined according to a previous report (De Boer and Noest, 1998) as follows:

$$\frac{d\mu_1}{dt} = 2p_1$$

$$\frac{d\mu_2}{dt} = 2p_2 - mR(\mu_2 - \mu_1 - K)$$

where p_1, p_2, m, and R are as above, K is the length of telomere loss upon clonal expansion in units of division, and μ_1 and μ_2 are the average number of divisions undergone by CD57⁻ and CD57⁺ memory T cells, respectively. The difference in telomere length between CD57⁻ and CD57⁺ memory T cells was estimated as:

$$\Delta = (\mu_2 - \mu_1)\,\varepsilon$$

where ε is the average number of base pairs (bp) lost per division (taken to be 50 bp [De Boer and Noest, 1998]), giving the following expression for the difference in telomere length:

$$\Delta_C = \varepsilon \left(\frac{2(p_2 - p_1)}{mR} + K \right)$$

Fitting procedure

The function $U(t)$ was fitted to the deuterium labeling data measured in saliva, and the free parameters f, ☐, and ☐ were estimated for each individual. The resulting parameterized $U(t)$ functions were then used as fixed inputs during simultaneous fitting of the deuterium labeling and telomere length data from CD57⁻ and CD57⁺ memory T cells using the equations for L_1, L_2, and Δ_C above. The free parameters were p_1, p_2, z_1, z_2, and mR. As telomerase is highly active during clonal expansion, the telomere length loss index (K) was initially set to 0 (Bodnar et al., 1996; Collins, 2006). This assumption was subsequently relaxed to explore the impact of variations in K (Figure S6). The contribution of self-renewal to the production of new CD57⁺ memory T cells was:

$$\text{contribution from self-renewal} = \frac{p_2 x_2}{p_2 x_2 + m x_1}$$

$$= \frac{p_2}{p_2 + mR}$$

To ensure that the labeling data and the telomere length data contributed equally to the fit, all residuals were normalized by the mean, and the deuterium residuals were divided by the number of labeling data points. Conclusions were analyzed for robustness against changes in the number of telomere base pairs lost per division. Scenarios in which CD57^{+} memory T cells did not proliferate were also tested by fixing p_2 to 0. Model performance was evaluated using the F test and the AICc (Burnham and Anderson, 2002). The model was fitted to the data using non-linear least squares regression implemented via the algorithm Pseudo in the FME package in R (Soetaert and Petzoldt, 2010).

DATA AND SOFTWARE AVAILABILITY

All datasets reported in this study are available on request from the Lead Contact, Kristin Ladell (ladellk@gmail.com).

$$\text{contribution from self-renewal} = \frac{p_2 x_2}{p_2 x_2 + m x_1}$$

ACKNOWLEDGEMENTS

AUTHOR CONTRIBUTIONS

M.K.H., J.M.M., D.A.P., D.C.M., and K.L. designed experiments; R.A., K.L.M., R.E.J., L.R., Y.Z., and K.L. performed experiments; C.B., M.K.H., J.M.M., D.M.B., D.A.P., D.C.M., and K.L. supervised experiments; R.A., K.L.M., R.E.J., L.R., D.M.B., D.C.M., and K.L. analyzed data; J.L.B. and B.A. modeled data; D.A.P., D.C.M., B.A., and K.L. wrote the manuscript. All authors contributed intellectually and approved the manuscript.

FIGURE LEGENDS

Figure 1. CD57$^-$ and CD57$^+$ memory T cells exhibit similar rates of deuterium incorporation. (A) Schematic representation of the ^{2}H$_2$O labeling protocol and sampling time points. (B) Experimental labeling data for CD57$^-$ and CD57$^+$ memory CD8$^+$ T cells sampled from the HIV-1-infected volunteers in Cohort 1. The corresponding flow cytometric gating strategy is shown in Figure S1. (C) Successive panels depict the flow cytometric gating strategy used to sort CD57$^-$ and CD57$^+$ memory T cells from the CD4$^+$ and CD8$^+$ lineages (Cohort 2). Lymphocytes were identified in a forward scatter-area versus side scatter-area plot, and single cells were identified in a forward scatter-area versus forward scatter-height plot. Boolean gates were drawn for analysis only to exclude fluorochrome aggregates. Viable CD3$^+$CD14$^-$CD19$^-$ cells were then identified in the CD4$^+$ and CD8$^+$ lineages, and sort gates were fixed on CD57$^-$ and CD57$^+$ memory cells after exclusion of potentially naive CD27^{bright}CD45RO$^-$ cells. (D) Experimental labeling data for CD57$^-$ and CD57$^+$ memory CD4$^+$ T cells sampled from the healthy volunteers in Cohort 2. (E) Experimental labeling data for CD57$^-$ and CD57$^+$ memory CD8$^+$ T cells sampled from the healthy volunteers in Cohort 2.

Figure 2. Ki67$^+$ cells are readily detectable in the CD57$^+$ memory T cell pool. (A) Representative flow cytometric data from a labeled volunteer (DW01) showing cytosolic expression of Ki67 among memory CD4$^+$ (top) or CD8$^+$ T cells (bottom) gated as CD57$^-$ (blue) or CD57$^+$ (red). (B) Percent cytosolic expression of Ki67 among memory CD4$^+$ (top) or CD8$^+$ T cells (bottom) gated as CD57$^-$ (blue triangles) or CD57$^+$ (red circles). *p < 0.05, **p < 0.01. Paired samples Wilcoxon test. (C) Representative flow cytometric data from unlabeled volunteers (n = 2) showing cytosolic/nuclear expression of Ki67 among memory CD4$^+$ T cells gated as CD57$^-$ (blue) or CD57$^+$ (red). HC07 was seronegative for CMV. (D) Top: percent cytosolic/nuclear expression of Ki67 among memory CD4$^+$ T cells gated as CD57$^-$ (blue triangles) or CD57$^+$ (red circles). Bottom: percent expression of CD28 among the corresponding Ki67$^+$CD57$^-$ (blue triangles) and Ki67$^+$CD57$^+$ memory CD4$^+$ T cells (red

circles). **p < 0.01. Paired samples Wilcoxon test. (E) Representative flow cytometric data from unlabeled volunteers (n = 2) showing cytosolic/nuclear expression of Ki67 among memory CD8$^+$ T cells gated as CD57$^-$ (blue) or CD57$^+$ (red). HC02 was seropositive for CMV, and HC08 was seronegative for CMV. (F) Top: percent cytosolic/nuclear expression of Ki67 among memory CD8$^+$ T cells gated as CD57$^-$ (blue triangles) or CD57$^+$ (red circles). Bottom: percent expression of CD28 among the corresponding Ki67$^+$CD57$^-$ (blue triangles) and Ki67$^+$CD57$^+$ memory CD8$^+$ T cells (red circles). *p < 0.05, **p < 0.01. Paired samples Wilcoxon test. (G) Phenotypic characteristics of Ki67$^+$CD57$^-$ and Ki67$^+$CD57$^+$ memory CD4$^+$ (top) or CD8$^+$ T cells (bottom) shown overlaid on density clouds representing the corresponding total CD4$^+$ (top) or CD8$^+$ T cell populations (bottom). Related to panel A. (H) Phenotypic characteristics of Ki67$^+$CD57$^-$ and Ki67$^+$CD57$^+$ memory CD4$^+$ T cells shown overlaid on density clouds representing the corresponding total CD4$^+$ T cell populations. Related to panel C. Key as in panel G. (I) Phenotypic characteristics of Ki67$^+$CD57$^-$ and Ki67$^+$CD57$^+$ memory CD8$^+$ T cells shown overlaid on density clouds representing the corresponding total CD8$^+$ T cell populations. Related to panel E. Key as in panel G.

Figure 3. CD57$^-$ and CD57$^+$ memory T cells have similar division histories. (A) Representative STELA data showing XpYp telomere lengths among CD57$^-$ and CD57$^+$ memory CD4$^+$ or CD8$^+$ T cells sampled from a labeled volunteer (DW02). (B) XpYp telomere lengths among CD57$^-$ and CD57$^+$ memory CD4$^+$ or CD8$^+$ T cells sampled from labeled volunteers (Cohort 2). *p < 0.05, **p < 0.01, ***p < 0.001. Mann-Whitney *U* test. (C) 17p telomere lengths among CD57$^-$ and CD57$^+$ memory CD4$^+$ or CD8$^+$ T cells sampled from unlabeled volunteers (Cohort 3). *p < 0.05, **p < 0.01, ***p < 0.001. Mann-Whitney *U* test. (D) Pooled XpYp telomere length data for the volunteers shown in panel B. Red lines show means with 95% confidence intervals. Mean values are specified above each column. Significance was assessed using the Mann-Whitney *U* test.

Figure 4. CD57$^-$ and CD57$^+$ memory T cells self-renew in vivo. (A) Schematic representation of the mathematical model. (B) Model fits to the measured data (dots) for CD57$^-$ and CD57$^+$ memory CD4$^+$ (left) or CD8$^+$ T cells (right) with p_2 constrained to zero (dashed lines) or free (solid lines).

REFERENCES

ABO, T. & BALCH, C. M. 1981. A differentiation antigen of human NK and K cells identified by a monoclonal antibody (HNK-1). *J Immunol*, 127**,** 1024–9.

ADDO, M. M., DRAENERT, R., RATHOD, A., VERRILL, C. L., DAVIS, B. T., GANDHI, R. T., ROBBINS, G. K., BASGOZ, N. O., STONE, D. R., COHEN, D. E., JOHNSTON, M. N., FLYNN, T., WURCEL, A. G., ROSENBERG, E. S., ALTFELD, M. & WALKER, B. D. 2007. Fully differentiated HIV-1 specific CD8+ T effector cells are more frequently detectable in controlled than in progressive HIV-1 infection. *PLoS One*, 2**,** e321.

AHMED, R., ROGER, L., COSTA DEL AMO, P., MINERS, K. L., JONES, R. E., BOELEN, L., FALI, T., ELEMANS, M., ZHANG, Y., APPAY, V., BAIRD, D. M., ASQUITH, B., PRICE, D.A., MACALLAN, D. C. & LADELL, K. 2016. Human stem cell-like memory T cells are maintained in a state of dynamic flux. *Cell Rep*, 17, 2811–8.

AHMED, R., WESTERA, L., DRYLEWICZ, J., ELEMANS, M., ZHANG, Y., KELLY, E., RELJIC, R., TESSELAAR, K., DE BOER, R., MACALLAN, D. C., BORGHANS, J. A. & ASQUITH, B. 2015. Reconciling estimates of cell proliferation from stable isotope labeling experiments. *PLoS Comput Biol*, 11**,** e1004355.

APPAY, V., VAN LIER, R. A., SALLUSTO, F. & ROEDERER, M. 2008. Phenotype and function of human T lymphocyte subsets: consensus and issues. *Cytometry A*, 73**,** 975–83.

BENITO, J. M., ORTIZ, M. C., LEÓN, A., SARABIA, L. A., LIGOS, J. M., MONTOYA, M., GARCIA, M., RUIZ-MATEOS, E., PALACIOS, R., CABELLO, A., RESTREPO, C., RODRIGUEZ, C., DEL ROMERO, J., LEAL, M., MUÑOZ-FERNÁNDEZ, M. A., ALCAMÍ, J., GARCÍA, F., GÓRGOLAS, M. & RALLÓN, N. 2018. Class-modeling analysis reveals T-cell homeostasis disturbances involved in loss of immune control in elite controllers. *BMC Med*, 16**,** 30.

BODNAR, A. G., KIM, N. W., EFFROS, R. B. & CHIU, C. P. 1996. Mechanism of telomerase induction during T cell activation. *Exp Cell Res*, 228**,** 58–64.

BRENCHLEY, J. M., KARANDIKAR, N. J., BETTS, M. R., AMBROZAK, D. R., HILL, B. J., CROTTY, L. E., CASAZZA, J. P., KURUPPU, J., MIGUELES, S. A., CONNORS, M., ROEDERER, M., DOUEK, D. C. & KOUP, R. A. 2003. Expression of CD57 defines replicative senescence and antigen-induced apoptotic death of CD8+ T cells. *Blood*, 101**,** 2711–20.

BURNHAM, K. P. & ANDERSON, D. R. 2002. Model selection and multimodel inference: a practical information-theoretic approach. 2nd Edition, Springer-Verlag, New York.

BUSCH, R., NEESE, R. A., AWADA, M., HAYES, G. M. & HELLERSTEIN, M. K. 2007. Measurement of cell proliferation by heavy water labeling. *Nat Protoc*, 2**,** 3045–57.

CAPPER, R., BRITT-COMPTON, B., TANKIMANOVA, M., ROWSON, J., LETSOLO, B., MAN, S., HAUGHTON, M. & BAIRD, D. M. 2007. The nature of telomere fusion and a definition of the critical telomere length in human cells. *Genes Dev*, 21**,** 2495–508.

CASAZZA, J. P., BETTS, M. R., PRICE, D. A., PRECOPIO, M. L., RUFF, L. E., BRENCHLEY, J. M., HILL, B. J., ROEDERER, M., DOUEK, D. C. & KOUP, R. A. 2006. Acquisition of direct antiviral effector functions by CMV-specific CD4+ T lymphocytes with cellular maturation. *J Exp Med*, 203**,** 2865–77.

CHATTOPADHYAY, P. K., BETTS, M. R., PRICE, D. A., GOSTICK, E., HORTON, H., ROEDERER, M. & DE ROSA, S. C. 2009. The cytolytic enzymes granzyme A, granzyme B, and perforin: expression patterns, cell distribution, and their relationship to cell maturity and bright CD57 expression. *J Leukoc Biol*, 85**,** 88–97.

CHONG, L. K., AICHELER, R. J., LLEWELLYN-LACEY, S., TOMASEC, P., BRENNAN, P. & WANG, E. C. 2008. Proliferation and interleukin 5 production by CD8hi CD57+ T cells. *Eur J Immunol*, 38**,** 995–1000.

COLLINS, K. 2006. The biogenesis and regulation of telomerase holoenzymes. *Nat Rev Mol Cell Biol*, 7**,** 484–94.

COSTA DEL AMO, P., LAHOZ-BENEYTEZ, J., BOELEN, L., AHMED, R., MINERS, K. L., ZHANG, Y., ROGER, L., JONES, R. E., MARRACO, S. A. F., SPEISER, D. E., BAIRD, D. M., PRICE, D. A., LADELL, K., MACALLAN, D. & ASQUITH, B. 2018. Human T$_{SCM}$ cell dynamics in vivo are compatible with long-lived immunological memory and stemness. *PLoS Biol*, 16**,** e2005523.

DAY, C. L., KAUFMANN, D. E., KIEPIELA, P., BROWN, J. A., MOODLEY, E. S., REDDY, S., MACKEY, E. W., MILLER, J. D., LESLIE, A. J., DEPIERRES, C., MNCUBE, Z., DURAISWAMY, J., ZHU, B., EICHBAUM, Q., ALTFELD, M., WHERRY, E. J., COOVADIA, H. M., GOULDER, P. J., KLENERMAN, P., AHMED, R., FREEMAN, G. J. & WALKER, B. D. 2006. PD-1 expression on HIV-specific T cells is associated with T-cell exhaustion and disease progression. *Nature*, 443**,** 350–4.

DE BOER, R. J. & NOEST, A. J. 1998. T cell renewal rates, telomerase, and telomere length shortening. *J Immunol*, 160**,** 5832–7.

FALI, T., FABRE-MERSSEMAN, V., YAMAMOTO, T., BAYARD, C., PAPAGNO, L., FASTENACKELS, S., ZOORAB, B., KOUP, R. A., BODDAERT, J., SAUCE, D. & APPAY, V. 2018. Elderly human hematopoietic progenitor cells express cellular senescence markers and are more susceptible to pyroptosis. *JCI Insight*, 3, e95319.

FREEMAN, G. J., WHERRY, E. J., AHMED, R. & SHARPE, A. H. 2006. Reinvigorating exhausted HIV-specific T cells via PD-1-PD-1 ligand blockade. *J Exp Med*, 203**,** 2223–7.

GERDES, J., SCHWAB, U., LEMKE, H. & STEIN, H. 1983. Production of a mouse monoclonal antibody reactive with a human nuclear antigen associated with cell proliferation. *Int J Cancer*, 31**,** 13–20.

GRATAMA, J. W., FRIDELL, E., LENKEI, R., OOSTERVEER, M. A., LJUNGSTROM, I., TANKE, H. J. & LINDE, A. 1989. Correlation between cytomegalovirus and Toxoplasma gondii serology and lymphocyte phenotypes in peripheral blood and cord blood. *Scand J Infect Dis*, 21, 611–6.

GUPTA, S. & GOLLAPUDI, S. 2007. Effector memory CD8$^+$ T cells are resistant to apoptosis. *Ann N Y Acad Sci*, 1109, 145–50.

HEGEDUS, A., NYAMWEYA, S., ZHANG, Y., GOVIND, S., ASPINALL, R., MASHANOVA, A., JANSEN, V. A., WHITTLE, H., JAYE, A., FLANAGAN, K. L. & MACALLAN, D. C. 2014. Protection versus pathology in aviremic and high viral load HIV-2 infection—the pivotal role of immune activation and T-cell kinetics. *J Infect Dis*, 210**,** 752–61.

HELLERSTEIN, M., HANLEY, M. B., CESAR, D., SILER, S., PAPAGEORGOPOULOS, C., WIEDER, E., SCHMIDT, D., HOH, R., NEESE, R., MACALLAN, D., DEEKS, S. & MCCUNE, J. M. 1999. Directly measured kinetics of circulating T lymphocytes in normal and HIV-1-infected humans. *Nat Med*, 5**,** 83–9.

IZQUIERDO, M., BALBOA, M. A., FERNANDEZ-RANADA, J. M., FIGUERA, A., TORRES, A., IRIONDO, A. & LOPEZ-BOTET, M. 1990. Relation between the increase of circulating CD3$^+$ CD57$^+$ lymphocytes and T cell dysfunction in recipients of bone marrow transplantation. *Clin Exp Immunol*, 82**,** 145–50.

KERN, F., KHATAMZAS, E., SUREL, I., FROMMEL, C., REINKE, P., WALDROP, S. L., PICKER, L. J. & VOLK, H. D. 1999. Distribution of human CMV-specific memory T cells among the CD8$^{pos.}$ subsets defined by CD57, CD27, and CD45 isoforms. *Eur J Immunol*, 29**,** 2908–15.

LADELL, K., HELLERSTEIN, M. K., CESAR, D., BUSCH, R., BOBAN, D. & MCCUNE, J. M. 2008. Central memory CD8$^+$ T cells appear to have a shorter lifespan and reduced abundance as a function of HIV disease progression. *J Immunol*, 180**,** 7907–18.

LAHOZ-BENEYTEZ, J., ELEMANS, M., ZHANG, Y., AHMED, R., SALAM, A., BLOCK, M., NIEDERALT, C., ASQUITH, B. & MACALLAN, D. 2016. Human neutrophil kinetics: modeling of stable isotope labeling data supports short blood neutrophil half-lives. *Blood*, 127**,** 3431–3438.

LE PRIOL, Y., PUTHIER, D., LECUREUIL, C., COMBADIERE, C., DEBRE, P., NGUYEN, C. & COMBADIERE, B. 2006. High cytotoxic and specific migratory potencies of

senescent CD8$^+$ CD57$^+$ cells in HIV-infected and uninfected individuals. *J Immunol*, 177**,** 5145–54.

MCCUNE, J. M., HANLEY, M. B., CESAR, D., HALVORSEN, R., HOH, R., SCHMIDT, D., WIEDER, E., DEEKS, S., SILER, S., NEESE, R. & HELLERSTEIN, M. 2000. Factors influencing T-cell turnover in HIV-1-seropositive patients. *J Clin Invest*, 105**,** R1–8.

MILLER, I., MIN, M., YANG, C., TIAN, C., GOOKIN, S., CARTER, D. & SPENCER, S. L. 2018. Ki67 is a graded rather than a binary marker of proliferation versus quiescence. *Cell Rep*, 24**,** 1105–12 e5.

NEESE, R. A., SILER, S. Q., CESAR, D., ANTELO, F., LEE, D., MISELL, L., PATEL, K., TEHRANI, S., SHAH, P. & HELLERSTEIN, M. K. 2001. Advances in the stable isotope-mass spectrometric measurement of DNA synthesis and cell proliferation. *Anal Biochem*, 298**,** 189–95.

NOCIARI, M. M., TELFORD, W. & RUSSO, C. 1999. Postthymic development of CD28$^-$ CD8$^+$ T cell subset: age-associated expansion and shift from memory to naive phenotype. *J Immunol*, 162**,** 3327–35.

NORTHFIELD, J. W., LOO, C. P., BARBOUR, J. D., SPOTTS, G., HECHT, F. M., KLENERMAN, P., NIXON, D. F. & MICHAELSSON, J. 2007. Human immunodeficiency virus type 1 (HIV-1)-specific CD8$^+$ T$_{EMRA}$ cells in early infection are linked to control of HIV-1 viremia and predict the subsequent viral load set point. *J Virol*, 81**,** 5759–65.

PATEL, A. A., ZHANG, Y., FULLERTON, J. N., BOELEN, L., RONGVAUX, A., MAINI, A. A., BIGLEY, V., FLAVELL, R. A., GILROY, D. W., ASQUITH, B., MACALLAN, D. & YONA, S. 2017. The fate and lifespan of human monocyte subsets in steady state and systemic inflammation. *J Exp Med*, 214**,** 1913–1923.

PETROVAS, C., CASAZZA, J. P., BRENCHLEY, J. M., PRICE, D. A., GOSTICK, E., ADAMS, W. C., PRECOPIO, M. L., SCHACKER, T., ROEDERER, M., DOUEK, D. C. & KOUP, R. A. 2006. PD-1 is a regulator of virus-specific CD8$^+$ T cell survival in HIV infection. *J Exp Med*, 203**,** 2281–92.

PETROVAS, C., CHAON, B., AMBROZAK, D. R., PRICE, D. A., MELENHORST, J. J., HILL, B. J., GELDMACHER, C., CASAZZA, J. P., CHATTOPADHYAY, P. K., ROEDERER, M., DOUEK, D. C., MUELLER, Y. M., JACOBSON, J. M., KULKARNI, V., FELBER, B. K., PAVLAKIS, G. N., KATSIKIS, P. D. & KOUP, R. A. 2009. Differential association of programmed death-1 and CD57 with ex vivo survival of CD8$^+$ T cells in HIV infection. *J Immunol*, 183**,** 1120–32.

PREVIS, S. F., HAZEY, J. W., DIRAISON, F., BEYLOT, M., DAVID, F. & BRUNENGRABER, H. 1996. Assay of the deuterium enrichment of water via acetylene. *J Mass Spectrom*, 31**,** 639–642.

RITCHIE, A. W., JAMES, K. & MICKLEM, H. S. 1983. The distribution and possible significance of cells identified in human lymphoid tissue by the monoclonal antibody HNK-1. *Clin Exp Immunol*, 51, 439–47.

SOETAERT, K. & PETZOLDT, T. 2010. Inverse modelling, sensitivity and Monte Carlo analysis in R using package FME. *J Stat Softw,* 33**,** 1–28.

TAKATA, H. & TAKIGUCHI, M. 2006. Three memory subsets of human CD8$^+$ T cells differently expressing three cytolytic effector molecules. *J Immunol*, 177**,** 4330–40.

TRAUTMANN, L., JANBAZIAN, L., CHOMONT, N., SAID, E. A., GIMMIG, S., BESSETTE, B., BOULASSEL, M. R., DELWART, E., SEPULVEDA, H., BALDERAS, R. S., ROUTY, J. P., HADDAD, E. K. & SEKALY, R. P. 2006. Upregulation of PD-1 expression on HIV-specific CD8$^+$ T cells leads to reversible immune dysfunction. *Nat Med*, 12**,** 1198–202.

VAN LEEUWEN, E. M., GAMADIA, L. E., BAARS, P. A., REMMERSWAAL, E. B., TEN BERGE, I. J. & VAN LIER, R. A. 2002. Proliferation requirements of cytomegalovirus-specific, effector-type human CD8$^+$ T cells. *J Immunol*, 169**,** 5838–43.

VERMA, K., OGONEK, J., VARANASI, P. R., LUTHER, S., BUNTING, I., THOMAY, K., BEHRENS, Y. L., MISCHAK-WEISSINGER, E. & HAMBACH, L. 2017. Human CD8$^+$ CD57$^-$ T$_{EMRA}$ cells: too young to be called "old". *PLoS One*, 12, e0177405.

VRISEKOOP, N., DRYLEWICZ, J., VAN GENT, R., MUGWAGWA, T., VAN LELYVELD, S. F., VEEL, E., OTTO, S. A., ACKERMANS, M. T., VERMEULEN, J. N., HUIDEKOPER, H. H., PRINS, J. M., MIEDEMA, F., DE BOER, R. J., TESSELAAR, K. & BORGHANS, J. A. 2015. Quantification of naive and memory T-cell turnover during HIV-1 infection. *AIDS*, 29**,** 2071–80.

WEGE, H., CHUI, M. S., LE, H. T., TRAN, J. M. & ZERN, M. A. 2003. SYBR Green real-time telomeric repeat amplification protocol for the rapid quantification of telomerase activity. *Nucleic Acids Res*, 31**,** E3–3.

WESTERA, L., ZHANG, Y., TESSELAAR, K., BORGHANS, J. A. & MACALLAN, D. C. 2013. Quantitating lymphocyte homeostasis in vivo in humans using stable isotope tracers. *Methods Mol Biol*, 979**,** 107–31.

ZHANG, Y., DE LARA, C., WORTH, A., HEGEDUS, A., LAAMANEN, K., BEVERLEY, P. & MACALLAN, D. 2013. Accelerated in vivo proliferation of memory phenotype CD4^{+} T-cells in human HIV-1 infection irrespective of viral chemokine co-receptor tropism. *PLoS Pathog*, 9**,** e1003310.

REAGENT or RESOURCE	SOURCE	IDENTIFIER
Stable isotope		
Heavy water (^2H_2O)	Cambridge Isotope Laboratories	Cat#DLM-4TPB-PK
Antibodies and fluorescent dyes		
LIVE/DEAD Fixable Aqua	Thermo Fisher Scientific	Cat#L34966
Anti-CD3–APC-H7 (clone SK7)	BD Biosciences	Cat#641415; RRID:NA
Anti-CD4–PE-Cy5.5 (clone S3.5)	Thermo Fisher Scientific	Cat#MHCD0418; RRID:AB_10376013
Anti-CD8–BV711 (clone RPA-T8)	BioLegend	Cat#301044; RRID:AB_2562906
Anti-CD14–V500 (clone M5E2)	BD Biosciences	Cat#561391; RRID:AB_10611856
Anti-CD19–V500 (clone HIB19)	BD Biosciences	Cat#561121; RRID:AB_10562391
Anti-CD27–QD605 (clone CLB-27/1)	Thermo Fisher Scientific	Cat#Q10065; RRID:AB_2556450
Anti-CD28–APC (clone CD28.2)	BD Biosciences	Cat#559770; RRID:AB_398666
Anti-CD28–BV421 (clone CD28.2)	BioLegend	Cat#302930; RRID:AB_2561910
Anti-CD45RA–PE (clone HI100)	BD Biosciences	Cat#555489; RRID:AB_395880
Anti-CD45RO–ECD (clone UCHL1)	Beckman Coulter	Cat#IM2712U; RRID:AB_10639537
Anti-CD57–FITC (clone NK-1)	BD Biosciences	Cat#555619; RRID:AB_395986
Anti-CD57–PE-Cy7 (clone NK-1)	BioLegend	Cat#359624; RRID:AB_2632689
Anti-CD127–BV421 (clone A019D5)	BioLegend	Cat#351310; RRID:AB_10960140
Anti-CCR7–PE-Cy7 (clone G043H7)	BioLegend	Cat#353226; RRID:AB_11126145
Anti-CXCR3–BV421 (clone G025H7)	BioLegend	Cat#353716; RRID:AB_2561448
Anti-Ki67–AF647 (clone B56)	BD Biosciences	Cat#558615; RRID:AB_647130
Anti-Ki67–FITC (clone B56)	BD Biosciences	Cat#556026; RRID:AB_396302
Anti-PD-1–BV421 (clone EH12.2H7)	BioLegend	Cat#329920; RRID:AB_10960742
Commercial buffer sets for flow cytometry		
Cytofix/Cytoperm Kit	BD Biosciences	Cat#554715
Foxp3 Transcription Factor Staining Buffer Kit	Thermo Fisher Scientific	Cat#00-5521-00
Chemicals		

Pentafluorobenzyl hydroxylamine	Sigma-Aldrich	Cat#194484
Sodium dodecyl sulphate	Thermo Fisher Scientific	Cat#10593355
Tris(hydroxymethyl) methylamine	Thermo Fisher Scientific	Cat#77-86-1
Ethylenediaminetetraacetic acid	Sigma-Aldrich	Cat#E6511-100G
Sodium hydroxide	Thermo Fisher Scientific	Cat#J/7620/15
Sodium phosphate dibasic	Sigma-Aldrich	Cat#7558-79-4
Hydrochloric acid	Thermo Fisher Scientific	Cat#7647-01-0
Commercial kits		
QIAmp DNA Mini Kit	Qiagen	Cat#51304
QIAmp DNA Micro Kit	Qiagen	Cat#56304
PCR reagents		
DreamTaq polymerase	Thermo Fisher Scientific	Cat#EP0702
Pwo polymerase	Sigma-Aldrich	Cat#11644955001
dNTPs	Promega	Cat#U1511
Oligonucleotides	Eurofins Genomics	Custom
Electrophoresis and hybridization		
Agarose MP	Sigma-Aldrich	Cat#11388983001
α-^{33}P dCTP	PerkinElmer	Cat#BLU013H100UC
Megaprime	VWR	Cat#RPN1607
Hybond-XL	VWR	Cat#RPN15205
Molecular weight markers		
1 kb ladder	Agilent	Cat#201115
2.5 kb ladder	Bio-Rad	Cat#1708205
Hardware		
FACSVantage SE	BD Biosciences	https://www.bdbiosciences.com
FACSAria	BD Biosciences	https://www.bdbiosciences.com
Special Order Research Product FACSAria II	BD Biosciences	https://www.bdbiosciences.com
GC/MS (5873/6980)	Agilent	https://www.agilent.com
DB-17 column	Agilent	Cat#122-4712
Tetrad2 Thermal Cycler	Bio-Rad	https://www.bio-rad.com
Typhoon FLA 9500 Phosphorimager	GE Healthcare	https://gelifesciences.com
Software		
DiVa version 8	BD	https://www.bdbiosciences.com

	Biosciences	
FlowJo software version 9.9.4	FlowJo LLC	https://www.flowjo.com
Phoretix 1D Quantifier	Nonlinear Dynamics	http://www.nonlinear.com/about/totallab
Prism version 8	GraphPad	https://www.graphpad.com

ID	p_1 (% per day)	SE (% per day)	z_1 (% per day)	SE (% per day)	p_2 (% per day)	SE (% per day)	z_2 (% per day)	SE (% per day)	mR (% per day)	SE (% per day)	Self-renewal (%)
CD4$^+$ T cells											
DW01	0.33	0.04	0.0088	0.27	0.59	0.08	1.24	0.37	0.02	0.01	97
DW02	0.65	0.06	1.89	0.31	2.08	0.23	3.77	0.58	0.17	0.03	93
DW04	0.53	ND	1.43	ND	0.53	ND	1.65	ND	0.00	ND	100
DW10	0.58	0.05	1.80	0.28	0.49	0.05	0.92	0.22	0.00	0.00	99
DW11	0.44	0.06	1.24	0.33	1.64	0.02	5.24	0.66	0.45	0.02	79
Median	**0.53**		**1.43**		**0.59**		**1.65**		**0.02**		**97**
CD8$^+$ T cells											
DW01	0.26	0.02	0.73	0.13	0.40	0.03	0.70	0.13	0.02	0.00	96
DW02	0.22	0.02	0.86	0.22	0.42	0.04	0.45	0.19	0.04	0.01	92
DW04	0.37	ND	0.91	ND	0.37	ND	0.62	ND	0.00	ND	100
DW10	0.55	0.17	3.60	1.53	0.34	0.11	0.63	0.56	0.02	0.02	95
DW11	0.07	0.01	0.24	0.34	0.32	0.03	0.81	0.04	0.07	0.01	83
Median	**0.26**		**0.86**		**0.37**		**0.63**		**0.02**		**95**

Table 1. Parameter estimates from model fits to the experimental data.

The best-fit estimates are shown. A limited number of data points were available from one volunteer (DW04). The asymptotic covariance matrix method was used to calculate standard errors. The percentage of new CD57$^+$ T cells generated via homeostatic proliferation (right column) was calculated as 100 x p_2 / (p_2 + mR). ND, not determined; SE, standard error.
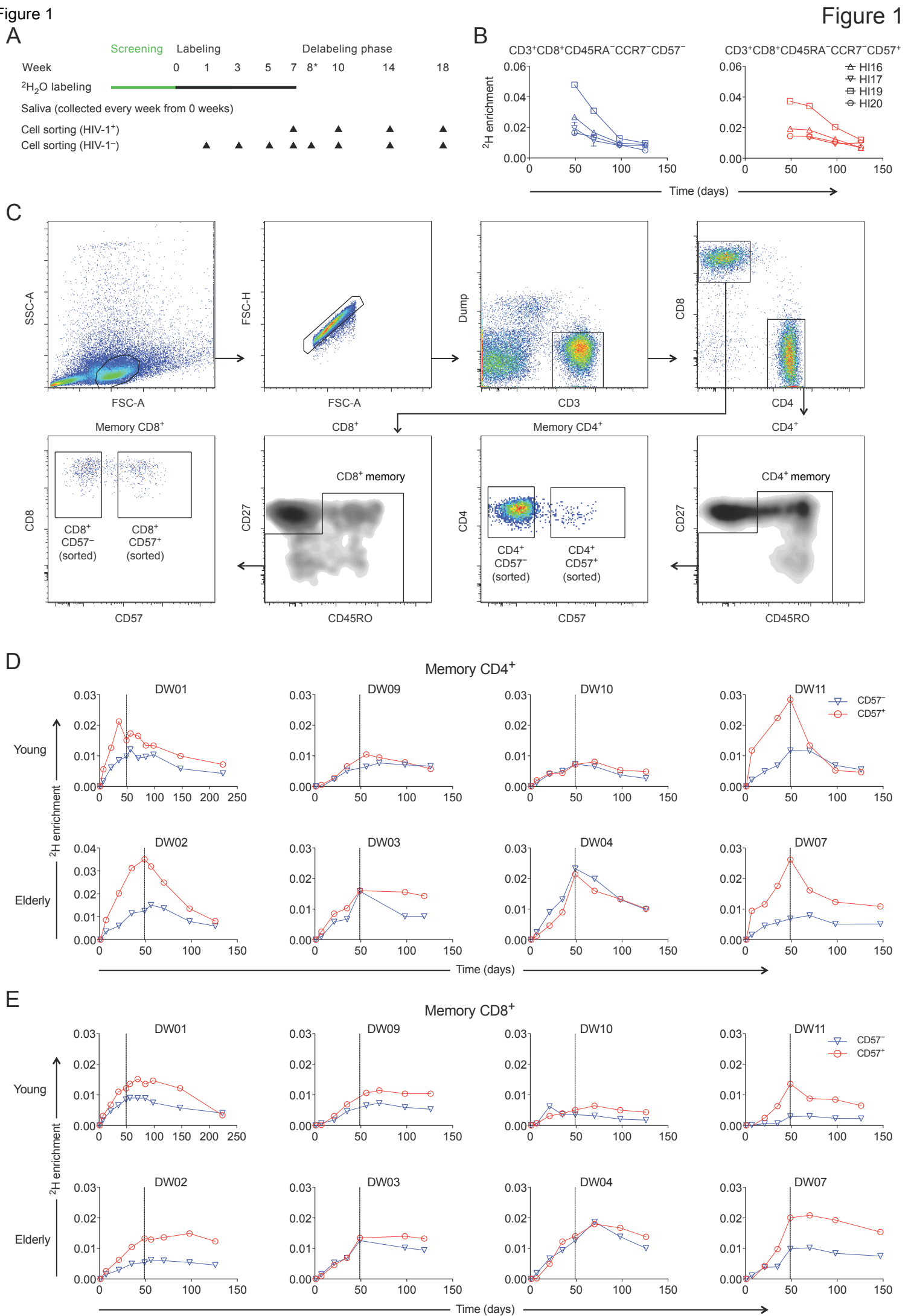
Figure 1
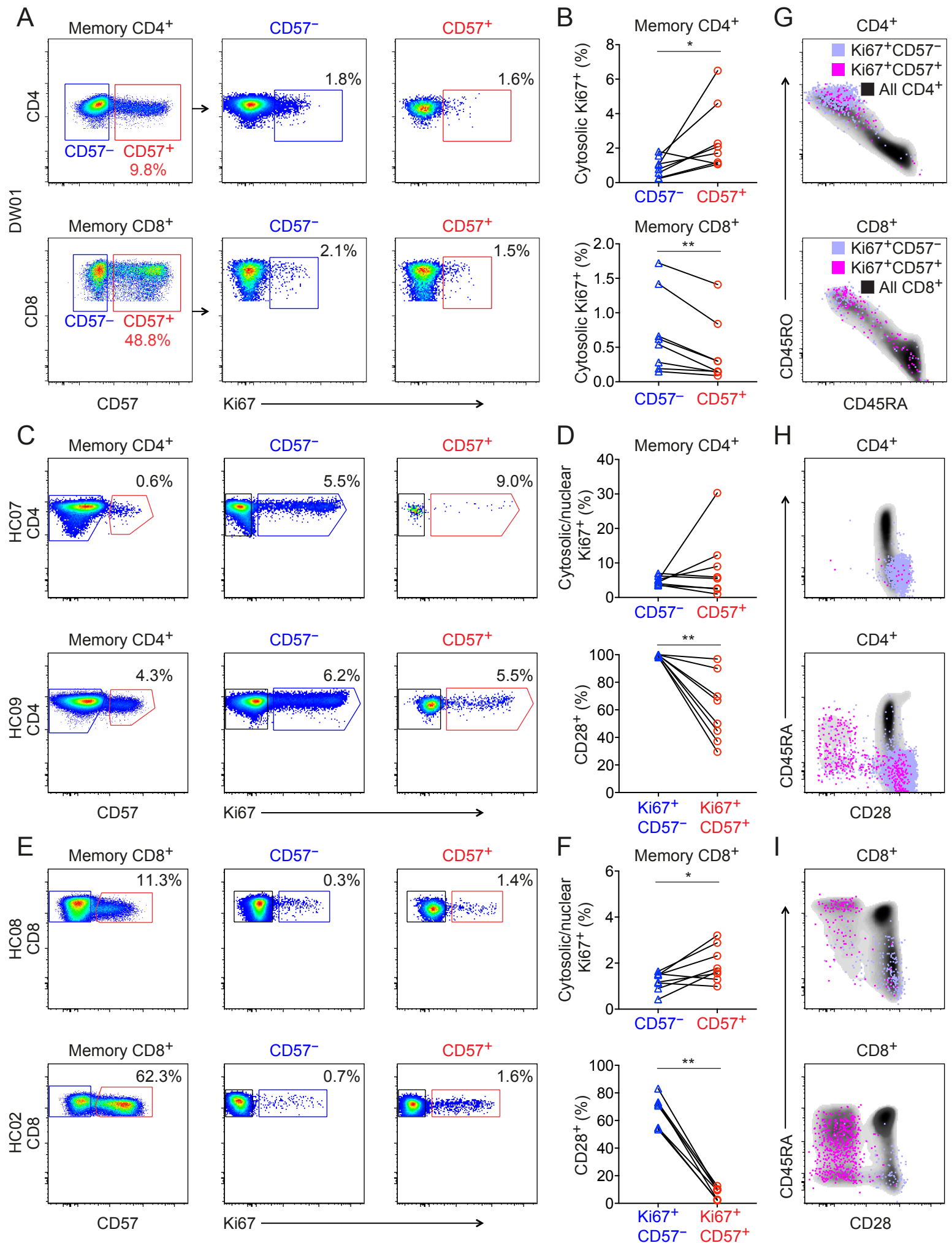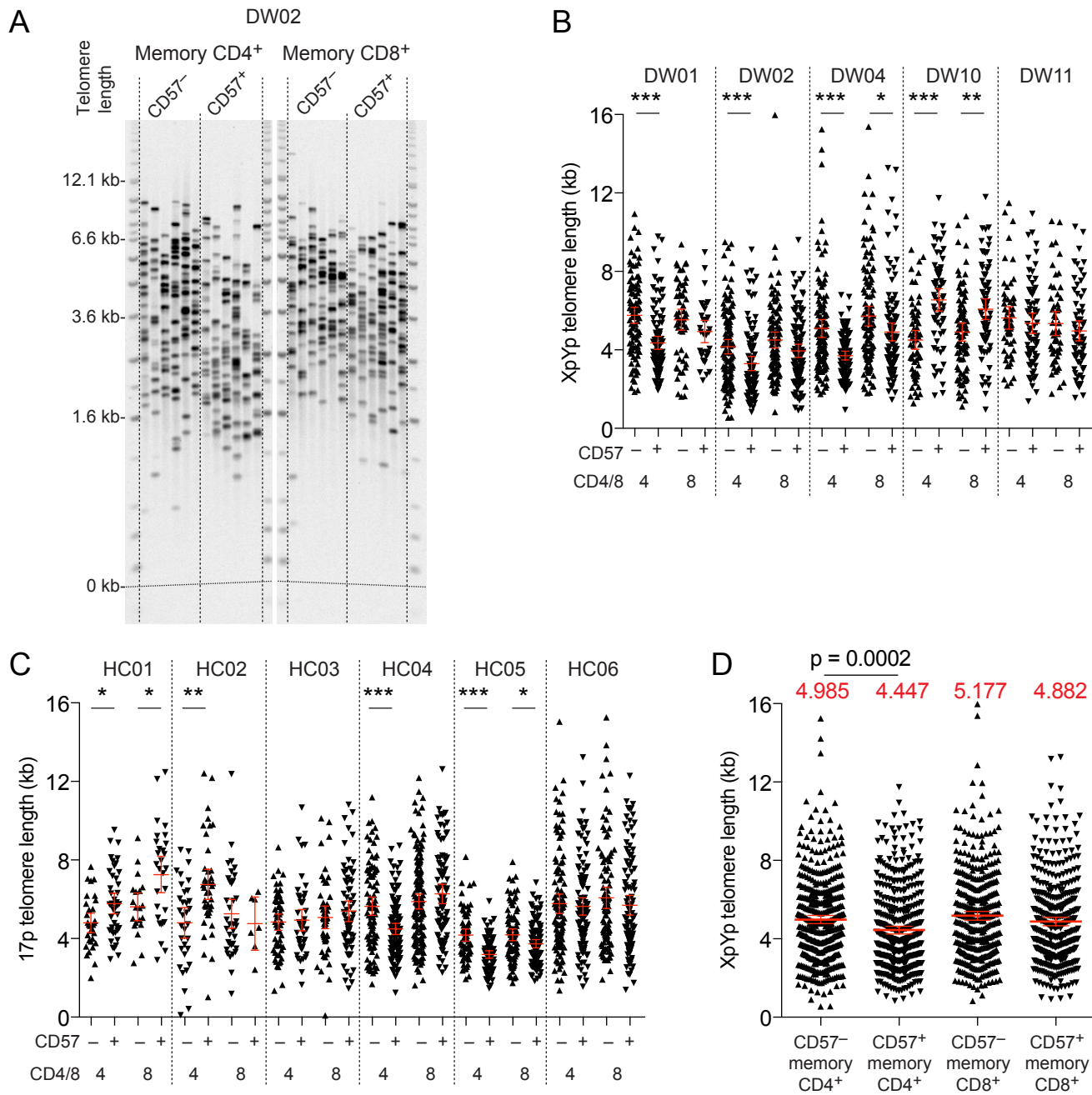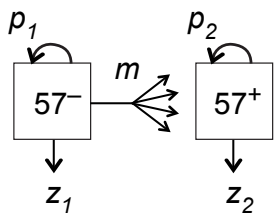
Figure 1

Figure 2

Figure 3

Figure 3

Figure 3
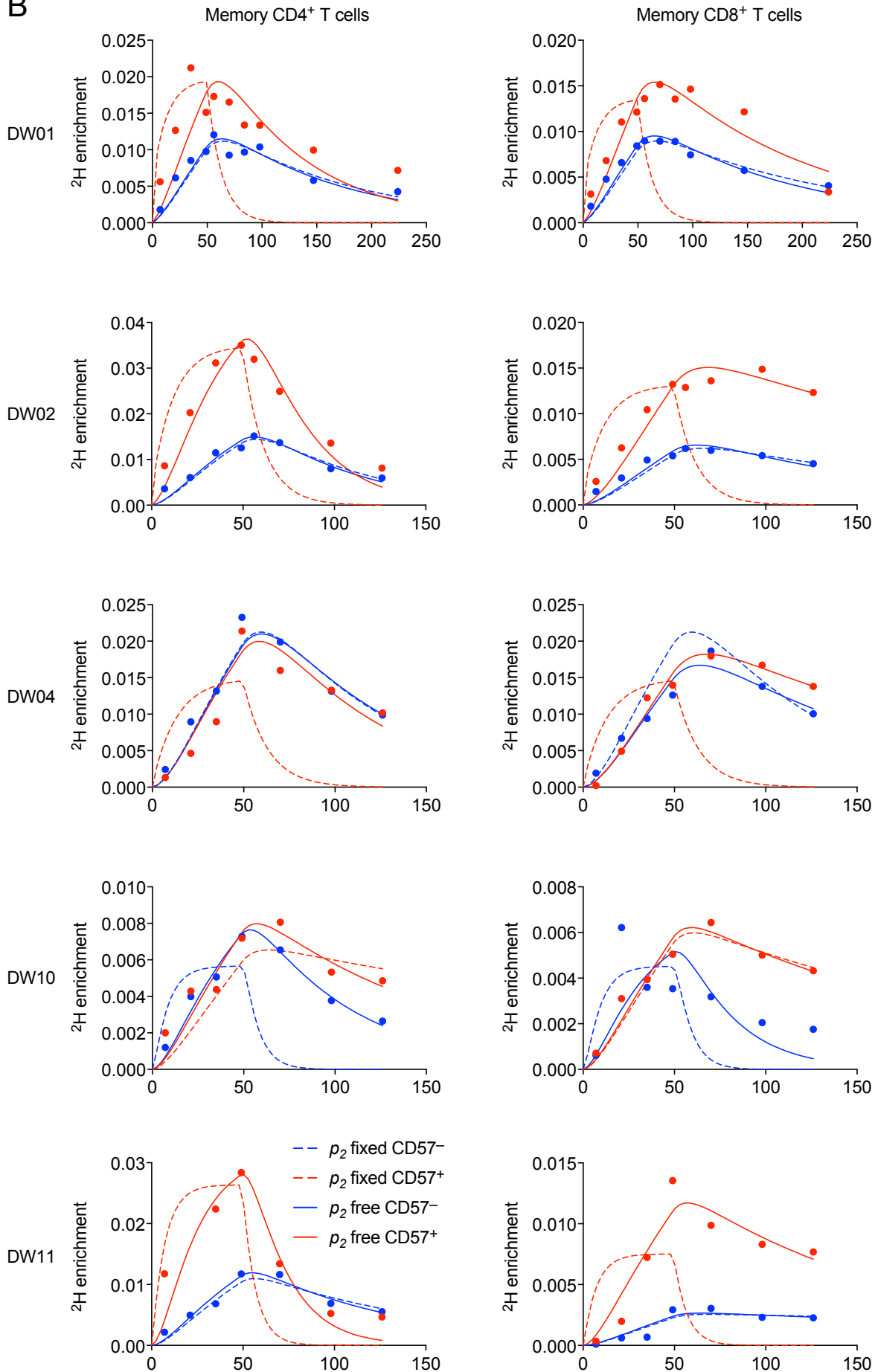
Figure 4

Figure 4

SUPPLEMENTAL MATERIAL

1. SUPPLEMENTAL FIGURES
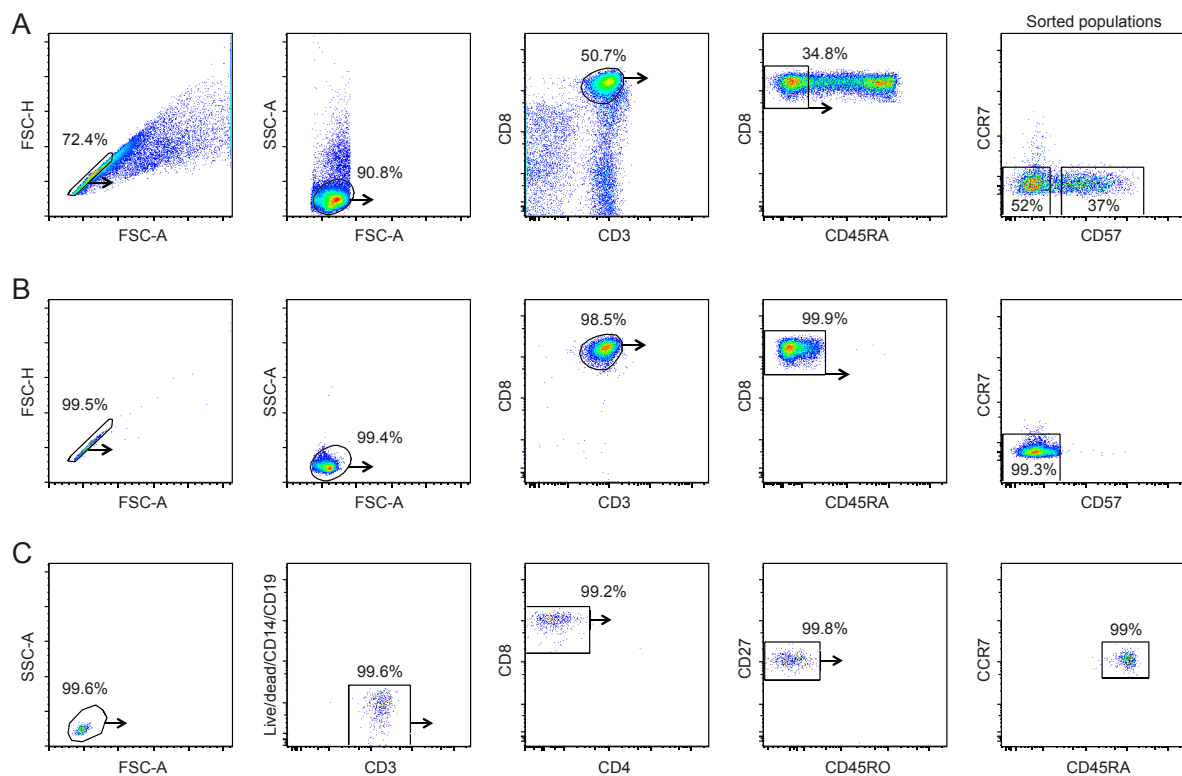
Figure S1. Flow cytometric gating strategy for the pilot ^{2}H$_2$O labeling study (Cohort 1) and representative sort purity checks (Cohorts 1 and 2). (A) Successive panels depict the flow cytometric gating strategy used to sort CD57$^-$ and CD57$^+$ memory CD8$^+$ T cells (Cohort 1). Single cells were identified in a forward scatter-area versus forward scatter-height plot, and lymphocytes were identified in a forward scatter-area versus side scatter-area plot. Sort gates were then fixed on CD3$^+$CD8$^+$CD45RA$^-$CCR7$^-$CD57$^-$ and CD3$^+$CD8$^+$CD45RA$^-$CCR7$^-$CD57$^+$ memory T cells. (B) Representative sort purity check for CD3$^+$CD8$^+$CD45RA$^-$CCR7$^-$CD57$^-$ memory T cells (Cohort 1). (C) Representative sort purity check for CD3$^+$CD8$^+$CD27$^+$CD45RO$^-$CCR7$^+$ naive T cells (Cohort 2). This abundant subset was analyzed to preserve CD57$^-$ and CD57$^+$ memory T cells. Related to Figure 1.
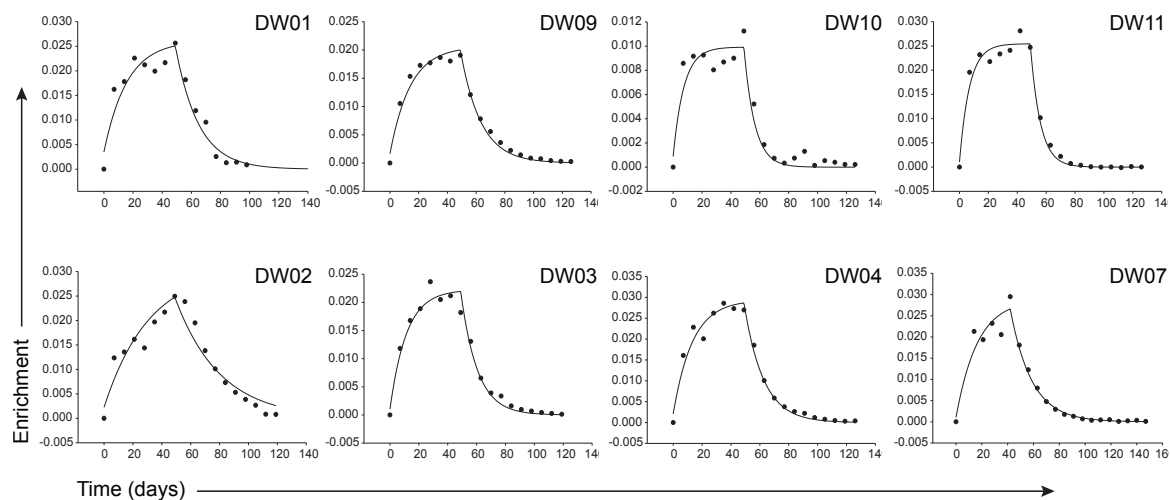
Figure S2. [2]H enrichment in body water. Measured ^{2}H enrichments in body water (dots) with best-fit curves (solid lines) for all volunteers in Cohort 2. Young volunteers are shown on the top row, and elderly volunteers are shown on the bottom row. Related to Figure 1.
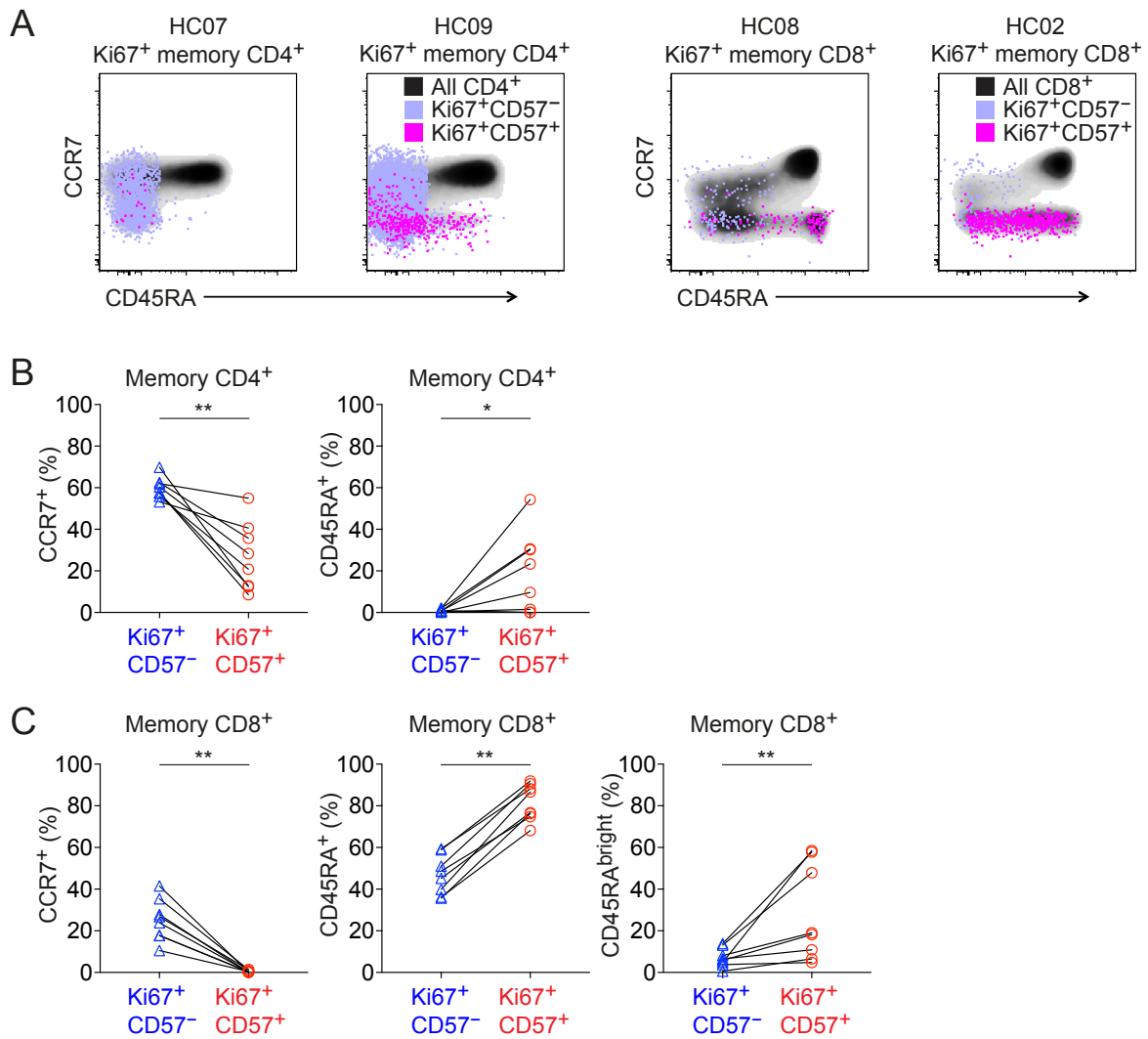
Figure S3. Expression of Ki67 among CD57$^-$ and CD57$^+$ memory T cells. (A) Representative flow cytometric data from unlabeled volunteers (n = 4) showing the phenotypic characteristics of Ki67$^+$CD57$^-$ and Ki67$^+$CD57$^+$ memory CD4$^+$ (left panels) or CD8$^+$ T cells (right panels) overlaid on density clouds representing the corresponding total CD4$^+$ (left panels) or CD8$^+$ T cell populations (right panels). HC02 was seropositive for CMV. HC07 and HC08 were seronegative for CMV. (B) Percent cytosolic/nuclear expression of CCR7 (left) and CD45RA (right) among Ki67$^+$CD57$^-$ (blue triangles) and Ki67$^+$CD57$^+$ memory CD4$^+$ T cells (red circles). (C) Percent cytosolic/nuclear expression of CCR7 (left) and CD45RA (center and right) among Ki67$^+$CD57$^-$ (blue triangles) and Ki67$^+$CD57$^+$ memory CD8$^+$ T cells (red circles). The right graph shows only CD45RA^{bright} events. *p < 0.05, **p < 0.01. Paired samples Wilcoxon test. Related to Figure 2.
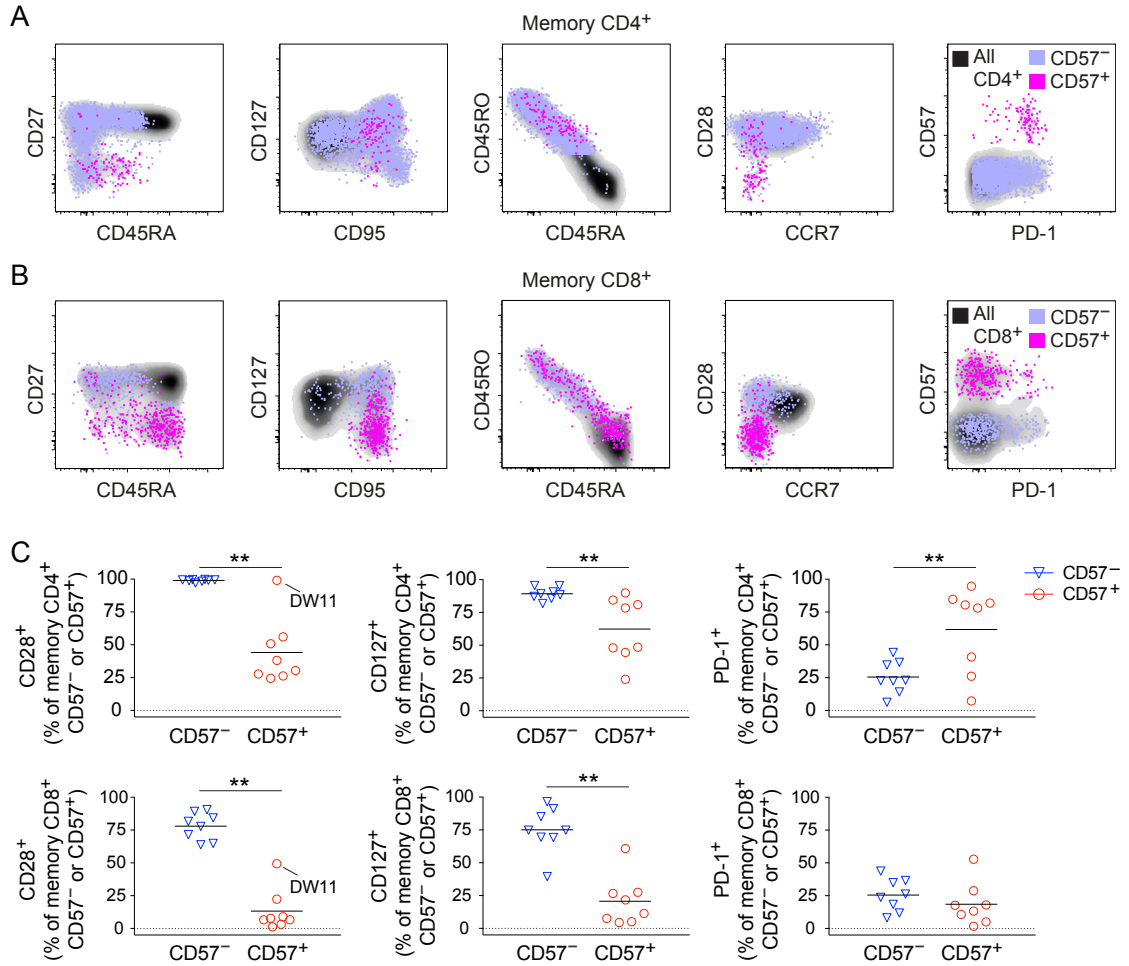
Figure S4. **CD57⁺ memory T cells are phenotypically distinct in the CD4⁺ and CD8⁺ lineages.** (A) Phenotypic characteristics of CD57$^-$ and CD57$^+$ memory CD4$^+$ T cells from a labeled volunteer (DW01) shown overlaid on density clouds representing the corresponding total CD4$^+$ T cell population. (B) Phenotypic characteristics of CD57$^-$ and CD57$^+$ memory CD8$^+$ T cells from a labeled volunteer (DW01) shown overlaid on density clouds representing the corresponding total CD8$^+$ T cell population. (C) Percent expression of CD28 (left), CD127 (center), and PD-1 (right) among CD57$^-$ and CD57$^+$ memory CD4$^+$ (top) or CD8$^+$ T cells (bottom) sampled from all volunteers in Cohort 2. Unusually high frequencies of CD57$^+$ memory CD4$^+$ and CD57$^+$ memory CD8$^+$ T cells expressed CD28 in one volunteer (DW11). **p < 0.01. Paired samples Wilcoxon test. Related to Figure 2.
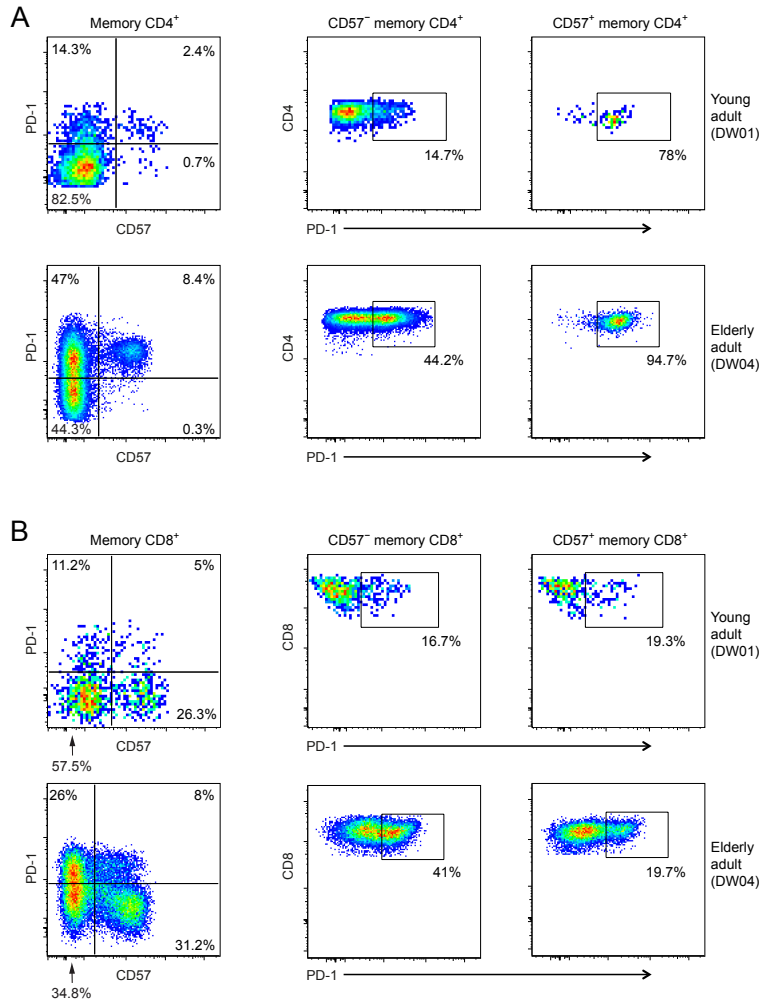
Figure S5. Expression of PD-1 among CD57⁻ and CD57⁺ memory T cells. (A) Representative flow cytometric data showing the expression of PD-1 among CD57⁻ and CD57⁺ memory CD4⁺ T cells. A young volunteer is shown on the top row (DW01). An elderly volunteer is shown on the bottom row (DW04). (B) Representative flow cytometric data showing the expression of PD-1 among CD57⁻ and CD57⁺ memory CD8⁺ T cells. A young volunteer is shown on the top row (DW01). An elderly volunteer is shown on the bottom row (DW04). Related to Figure 2.
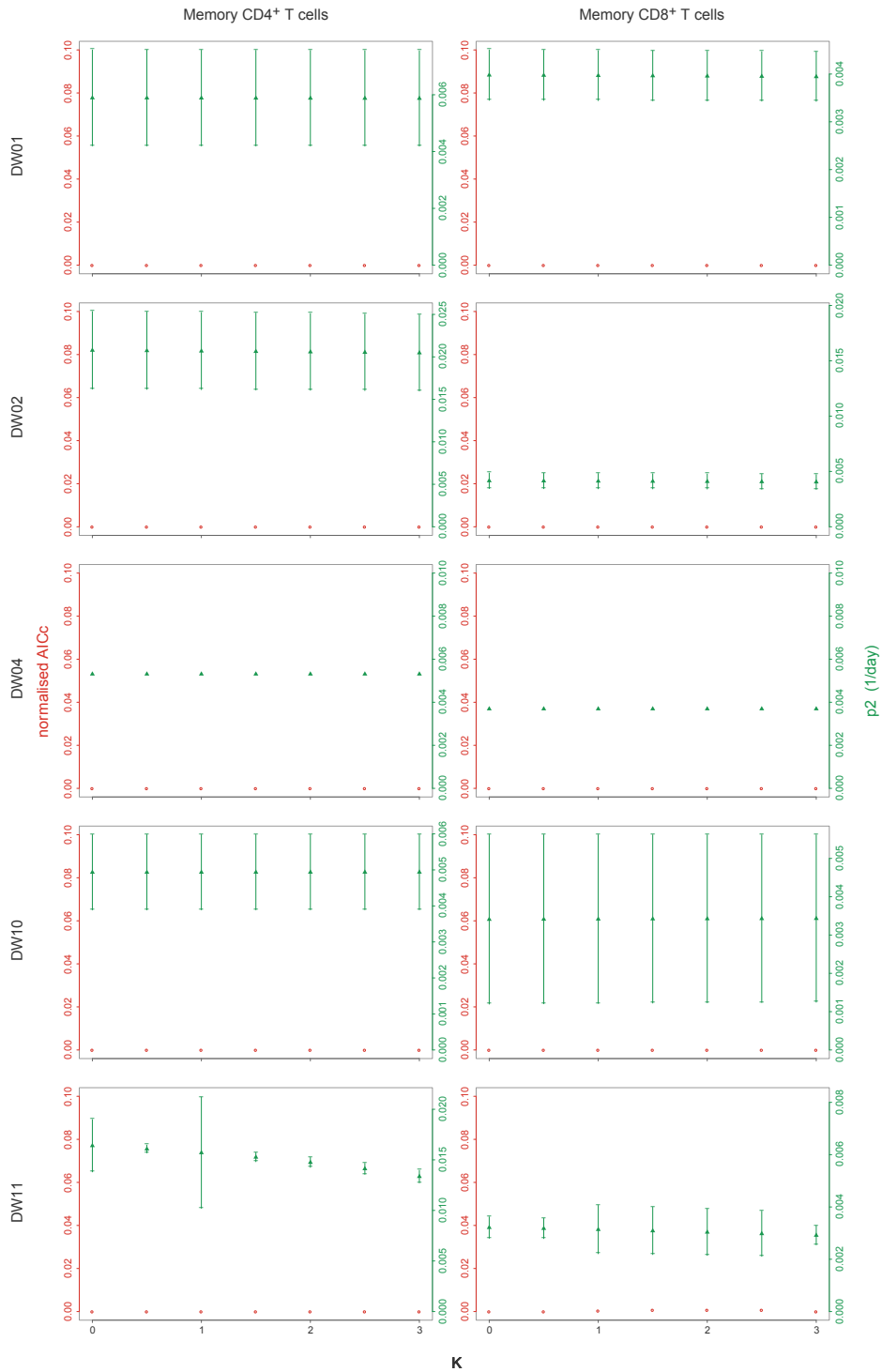
Figure S6. Sensitivity of parameter estimates and AICc values to changes in the telomere loss index shift (*K*). The telomere loss index shift, defined as the length of telomere lost per unit of division, is shown on the x-axes (denoted as *K*). Each plot shows the impact of varying *K* on the normalized AICc (red circles) and the estimated rate of proliferation in the corresponding CD57^{+} memory T cell population (green triangles). Error bars show 95% confidence intervals. Normalized AICc = AICc − AICc of the winning model. Related to Figure 4.
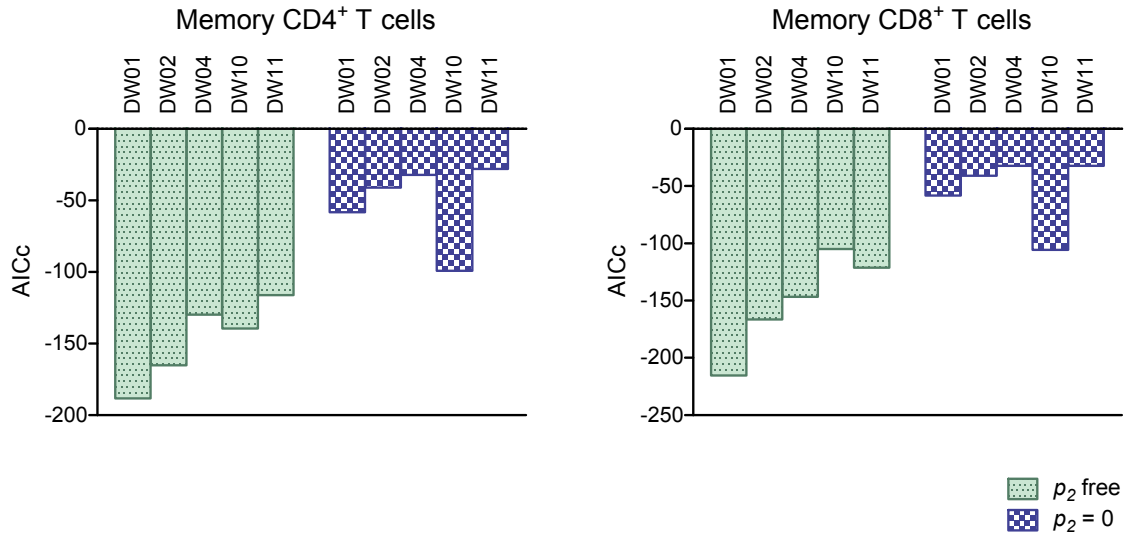
Figure S7. Quality of model fits to the experimental data with p_2 free or constrained to zero. Quality of fit was assessed using the AICc. Lower values indicate a better quality of fit, and higher values indicate a worse quality of fit. The proliferation rate in each CD57^{+} memory T cell population (p_2) was either free (green) or constrained to zero (blue). Related to Figure 4.

2. SUPPLEMENTAL TABLES

ID	Age	Gender	HIV-1 load (copies/mL plasma)	CD4$^+$ T cell count (x10^9/L)	CD8$^+$ T cell count (x10^9/L)	CMV serology	HIV-1 serology
HI16	53	Male	74,199	0.330	1.397	+	+
HI17	40	Male	2,059	0.852	3.388	+	+
HI19	36	Male	448,343	0.349	2.445	+	+
HI20	38	Male	30,851	0.431	1.646	+	+
DW01	32	Female	NA	0.809	0.460	+	–
DW02	64	Male	NA	0.681	0.314	+	–
DW03	78	Male	NA	0.869	0.405	+	–
DW04	83	Male	NA	0.885	0.579	+	–
DW07	60	Female	NA	0.654	0.241	+	–
DW09	47	Male	NA	1.077	0.800	+	–
DW10	34	Male	NA	0.488	0.977	+	–
DW11	29	Female	NA	1.380	0.864	+	–

Table S1. Clinical details and demographics of HIV-1-infected (HI) and healthy volunteers (DW) included in the labeling studies. NA, not applicable.